AEM
Journals.ASM.org

Hierarchy in Pentose Sugar Metabolism in *Clostridium acetobutylicum*

Ludmilla Aristilde,[a,b] Ian A. Lewis,[b]* Junyoung O. Park,[c] Joshua D. Rabinowitz[b,d]

Department of Biological and Environmental Engineering, College of Agricultural and Life Sciences, Cornell University, Ithaca, New York, USA[a]; Lewis-Sigler Institute for Integrative Genomics, Princeton University, Princeton, New Jersey, USA[b]; Department of Chemical and Biological Engineering, Princeton, New Jersey, USA[c]; Department of Chemistry, Princeton University, Princeton, New Jersey, USA[d]

Bacterial metabolism of polysaccharides from plant detritus into acids and solvents is an essential component of the terrestrial carbon cycle. Understanding the underlying metabolic pathways can also contribute to improved production of biofuels. Using a metabolomics approach involving liquid chromatography-mass spectrometry, we investigated the metabolism of mixtures of the cellulosic hexose sugar (glucose) and hemicellulosic pentose sugars (xylose and arabinose) in the anaerobic soil bacterium *Clostridium acetobutylicum*. Simultaneous feeding of stable isotope-labeled glucose and unlabeled xylose or arabinose revealed that, as expected, glucose was preferentially used as the carbon source. Assimilated pentose sugars accumulated in pentose phosphate pathway (PPP) intermediates with minimal flux into glycolysis. Simultaneous feeding of xylose and arabinose revealed an unexpected hierarchy among the pentose sugars, with arabinose utilized preferentially over xylose. The phosphoketolase pathway (PKP) provides an alternative route of pentose catabolism in *C. acetobutylicum* that directly converts xylulose-5-phosphate into acetyl-phosphate and glyceraldehyde-3-phosphate, bypassing most of the PPP. When feeding the mixture of pentose sugars, the labeling patterns of lower glycolytic intermediates indicated more flux through the PKP than through the PPP and upper glycolysis, and this was confirmed by quantitative flux modeling. Consistent with direct acetyl-phosphate production from the PKP, growth on the pentose mixture resulted in enhanced acetate excretion. Taken collectively, these findings reveal two hierarchies in clostridial pentose metabolism: xylose is subordinate to arabinose, and the PPP is used less than the PKP.

Clostridium is a genus of ubiquitous soil-dwelling obligate anaerobic bacteria that play an important role in the terrestrial carbon cycle. These bacteria ferment polysaccharides from plant detritus, including sugars from cellulose and hemicellulose, into acids and solvents (1–5). The model organism *Clostridium acetobutylicum* and other *Clostridium* species are of considerable commercial interest because of their ability to produce hydrogen gas, acetone, butanol, and ethanol from lignocellulosic components (6–8). Elucidating the metabolic pathways and regulatory mechanisms controlling polysaccharide metabolism is a critical step toward understanding anaerobic plant matter degradation in soils and harnessing this pathway for industrial-scale biofuel production (9).

The most common polysaccharides in plant detritus are cellulose and hemicellulose. Cellulose is a polymer of glucose (Gluc), whereas hemicellulose, the second most abundant component of plant cell walls, is composed primarily of the pentose sugars xylose (Xyl) and arabinose (Arab) (Fig. 1A) (9). Efficient utilization of plant biomass thus requires the metabolism of both hexose and pentose sugars. In *C. acetobutylicum*, Gluc is metabolized via glycolysis to supply energy requirements and carbon demands from the nonoxidative pentose phosphate pathway (PPP), amino acid biosynthesis, acidogenic and solventogenic pathways, and the tricarboxylic acid cycle (Fig. 1B) (10–12). Historically, it was assumed that carbons from Xyl and Arab pass from the PPP through glycolysis to supply acidogenesis and solventogenesis. However, two recent studies (5, 13) reported that acids and solvents can be produced from these sugars from a glycolysis-independent pathway, the phosphoketolase pathway (PKP) (Fig. 1B). The PKP involves cleavage of xylulose-5-phosphate (Xu5P) into glyceraldehyde-3-phosphate (GAP) and acetyl-phosphate (Ac-P) and, to a lesser extent, cleavage of fructose-6-phosphate (F6P) into erythrose-4-phosphate (E4P) and Ac-P (Fig. 1B) (5, 13). The metabolite Ac-P is a direct precursor to either acetate or acetyl coenzyme A (acetyl-CoA), which are both involved in clostridial production of acids and solvents (Fig. 1B). Using ^{13}C metabolic flux analysis, Liu et al. (13) calculated that Xyl catabolic flux through the PKP in *C. acetobutylicum* increases with increasing Xyl concentration. Furthermore, due to both higher ratios of excreted acetate and a more than 100-fold increase in the mRNA expression of the phosphoketolase enzyme in the presence of Arab, Servinsky et al. (5) proposed that the PKP is more significant when the cells are grown with Arab as the C source than with either Gluc or Xyl. However, the significance of this pathway in the metabolism of sugar mixtures was not elucidated.

Previous reports imply that metabolic regulation may control the differential utilization of hexose versus pentose sugars. Although *C. acetobutylicum* can metabolize either Gluc or Xyl individually, Xyl metabolism is severely inhibited when Gluc is available (14–17). The overexpression of an *Escherichia coli* transaldolase-encoding gene, *talA*, in *C. acetobutylicum* increased Xyl utilization when the pentose sugar was the sole source of car-

Received 21 October 2014 **Accepted** 11 December 2014

Accepted manuscript posted online 19 December 2014

Citation Aristilde L, Lewis IA, Park JO, Rabinowitz JD. 2015. Hierarchy in pentose sugar metabolism in *Clostridium acetobutylicum*. Appl Environ Microbiol 81:1452–1462. doi:10.1128/AEM.03199-14.

Editor: R. M. Kelly

Address correspondence to Ludmilla Aristilde, ludmilla@cornell.edu, or Joshua D. Rabinowitz, joshr@genomics.princeton.edu.

* Present address: Ian A. Lewis, Department of Biological Sciences, University of Calgary, Calgary, Alberta, Canada.

Supplemental material for this article may be found at http://dx.doi.org/10.1128/AEM.03199-14.

doi:10.1128/AEM.03199-14

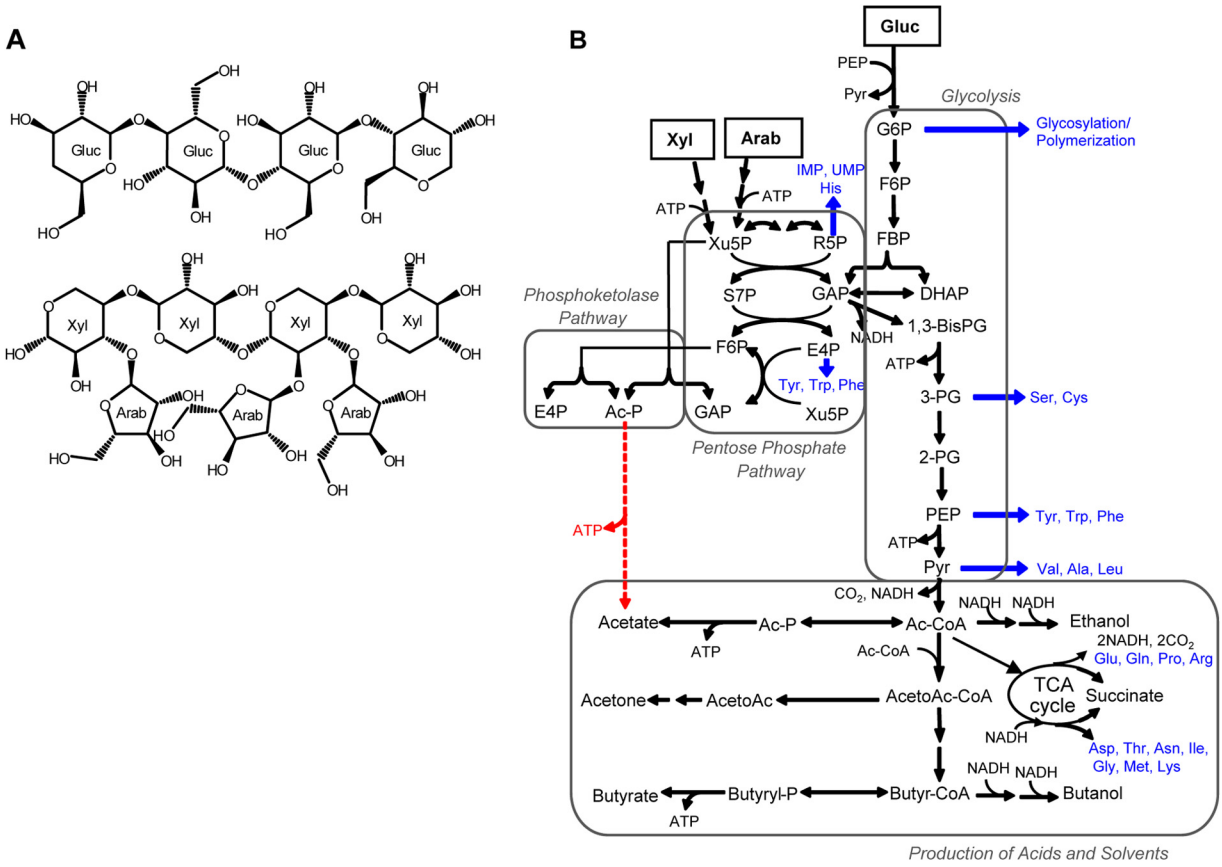

FIG 1 (A) Structure of polymers from cellulose and hemicellulose: cellulodextrins (top) is composed of repeated β-1,4-linked D-glucose (Gluc) dimers or cellobiose units, and arabinoxylan (bottom) is a polymer of β-1,4-linked D-xylose (Xyl) monomers substituted with L-arabinose (Arab) at the 2, 3, or 2,3 positions. (B) Schematic of the central carbon metabolism of *C. acetobutylicum* showing the point of entry of the different sugars and the major catabolic pathways in black, including glycolysis, the pentose phosphate pathway, and the phosphoketolase pathway, with the anabolic pathways toward biomass production shown in blue. Glucose-6-phosphate, G6P; fructose-6-phosphate, F6P; fructose-1,6-bisphosphate, FBP; dihydroxyacetone-phosphate, DHAP; glyceraldehyde-3-phosphate, GAP; xylulose-5-phosphate, Xu5P; ribose-5-phosphate, R5P; sedoheptulose-7-phosphate, S7P; erythrose-4-phosphate, E4P; acetyl-P, Ac-P; IMP; UMP; 1,3-bisphosphoglycerate, 1,3-BisPG; 3-phosphoglycerate, 3-PG; 2-phosphoglycerate, 2-PG; phosphoenolpyruvate, PEP; pyruvate, Pyr; acetyl-CoA, Ac-CoA; acetoacetyl-CoA, AcetoAc-CoA; butyryl-CoA, Butyr-CoA; and amino acids are shown as their 3-letter codes.

bon (18); the transaldolase reaction mediates the formation of E4P and F6P, a glycolytic intermediate, by combining two PPP intermediates, GAP and sedoheptulose-7-phosphate (S7P) (Fig. 1B). However, in mixtures of Gluc and Xyl in solution (Gluc:Xyl), the overexpressed strain still exhibited low Xyl consumption (18). These observations suggest a regulatory mechanism that enables Gluc-mediated repression of Xyl metabolism (18). In contrast, it was shown recently that a new *Clostridium* strain (BOH3) was capable of utilizing Gluc and Xyl simultaneously (19). This capability was attributed to the lack of significant repression of Xyl isomerase and xylulose kinase in this strain in the presence of Gluc (19). On the other hand, in *C. acetobutylicum*, Grimmler et al. (15) reported that the expression of enzymes involved in Xyl metabolism in the PPP (Xyl transporter, xylulose kinase, transketolase, and transaldolase) was downregulated in the presence of Gluc. Disrupting the gene encoding Ccpa, a key protein shown to be involved in Gluc-mediated repression of the utilization of other carbon sources in *Bacillus* species (20–22), has led to improved mixed-sugar utilization by *C. acetobutylicum* (5). Similarly, disrupting *glcG*, which encodes part of the Gluc phosphoenolpyruvate-dependent phosphotransferase system for Gluc uptake, resulted in upregulation of genes involved in Xyl and Arab catabolism and thus improved pentose utilization in media containing mixtures of Gluc and pentose sugars (23).

These previous findings thus indicated that *C. acetobutylicum* metabolizes hexose sugars preferentially over pentose sugars and, to circumvent catabolite repression by Gluc in mixtures, increase in PPP enzymes, increase in pentose uptake enzymes, and/or decrease in Gluc-mediated signaling was necessary. The metabolic fate of carbons from mixed-sugar sources has, however, not been determined. Recent advances in liquid chromatography-mass spectrometry (LC-MS) and nuclear magnetic resonance (NMR) spectroscopy have made metabolomics a powerful approach for investigating the activity and regulation of complex metabolic networks (10, 11, 24–28, 30, 43). In the present study, we employed a metabolomics approach and a quantitative metabolic flux analysis (MFA) to investigate the hierarchy in the utilization of hemicellulosic pentose sugars by *C. acetobutylicum* in the presence and absence of Gluc. In addition to a preference for glucose over pentose sugars for feeding pathways other than the PPP, we find a preference for arabinose over xylose. Moreover, we show that the PKP is used preferentially over the PPP in catabolizing the

pentose sugars. Our findings provide insights into the metabolic fate of different sugar substrates, which may provide a foundation toward enhancing clostridial biofuel production from sugar mixtures.

MATERIALS AND METHODS

Materials. Freeze-dried cultures of *C. acetobutylicum* (strain 824) were obtained from ATCC. Isotopically labeled compounds were purchased from Cambridge Isotopes or Omicron Biochemicals; all other chemicals were obtained from Fisher or Sigma-Aldrich (analytical grade). All experiments were conducted inside a Bactron IV SHEL LAB anaerobic chamber, with an atmosphere of 90% N_2, 5% H_2, and 5% CO_2. An oxygen sensor inside the chamber constantly monitored the O_2 level to ensure anaerobic conditions were maintained.

Growth conditions. To prepare for the batch growth experiments, *C. acetobutylicum* single colonies were picked from agar-solidified reinforced clostridial medium (RCM; Difco), resuspended in substrate-rich RCM medium, and heat-treated at 80°C for 20 min. All subsequent growth was conducted in the anaerobic environmental chamber (see above) at 37°C. Cells were grown to saturation overnight in the rich medium before inoculation (1:100 dilution) in a liquid minimal medium at an initial optical density at 600 nm (OD_{600}) of 0.05. When this liquid culture reached mid-exponential phase (OD_{600} of 0.5 to 0.8), it was used to reinoculate (1:10) a fresh minimal medium (100 ml) used to conduct the experiments in a 250-ml Erlenmeyer flask. The minimal medium consists of a previous recipe (27) supplemented with trace mineral components: 14.7 mM KH_2PO_4, 11.5 mM K_2HPO_4, 0.81 mM $MgSO_4 \cdot 7H_2O$, 28.0 mM NH_4Cl, 1.6 mM $CaCl_2 \cdot 2H_2O$, 52.7 μM $FeSO_4 \cdot 7H_2O$, 16.0 nM $CuSO_4 \cdot 2H_2O$, 0.80 nM $MnCl_2$, 1.46 μM $CoCl_2$, 0.15 nM $Na_2MoO_4 \cdot 2H_2O$, 89.8 nM $NiSO_4 \cdot 2H_2O$, 0.26 nM $ZnCl_2$, 48.5 nM H_3BO_3, 532 nM biotin, and 1.17 μM 4-aminobenzoic acid. The concentration of each sugar in the minimal medium was 333 mmol C $liter^{-1}$ (e.g., for a six-carbon sugar, 55.5 mmol $liter^{-1}$ or 10 g $liter^{-1}$ Gluc). We performed experiments with Gluc, Gluc:Xyl, Gluc:Arab, and Xyl:Arab with equal molar amounts of C of each sugar. To monitor the differential incorporation of assimilated sugars into intracellular metabolites of glycolysis and PPP, long-term isotopic enrichment was achieved by growing *C. acetobutylicum* for at least 4 h during exponential growth in minimal medium with the following substrates: [U-$^{13}C_6$]Gluc alone and with unlabeled Arab or unlabeled Xyl, and [1,2-$^{13}C_2$]Xyl alone and with unlabeled Arab. As the labeling halftime of the measured metabolites is less than 30 min (11), 4 h constitutes at least 8 labeling half-times, and accordingly these long-term isotopic enrichment measurements approximate steady-state labeling.

Measurements of sugars and metabolites. For the quantitation of sugar and fermentation products (i.e., butyrate, acetate, butanol, acetone, and ethanol) in the extracellular medium, we harvested medium samples throughout the growth of *C. acetobutylicum* under each condition by filtering an aliquot (2 ml) of the culture through nylon filters (0.22-μm pore size) and storing the filtrate at −80°C until NMR analysis. NMR samples were prepared in 10% D_2O with 500 μM NaN_3 as an antimicrobial agent and 500 μM DSS (2,2-dimethyl-2-silapentane-5-sulfonate) as a chemical shift reference compound. Medium components were identified and quantified by one-dimensional ^{1}H NMR spectroscopy. Water signals were suppressed with excitation sculpting (32), and spectra were acquired in 4 transients, with a 1-s recycle delay and a 4-s acquisition. Spectra were zero-filled, Fourier-transformed with line broadening of 1 Hz, and phased in TopSpin. Metabolites were identified and quantified using the rNMR software package following established methods (33). Metabolite standards were used to identify diagnostic resonances for each compound and to calibrate concentration versus NMR intensity curves. The depletion of sugar in the extracellular medium was taken to equate the sugar consumption as done previously (10). Kinetic isotopic corporation of labeled substrates confirmed that this assumption was valid (see Fig. S1 in the supplemental material).

To characterize the intracellular metabolome, cells from 3 ml of exponentially growing cultures were collected on nylon filters (0.45-μm pore size), and metabolites were extracted from the cells by immediately submerging filters in 2 ml of −20°C acetonitrile-methanol-water (40:40:20) (34, 46). Extracts were centrifuged and the supernatant solutions were analyzed by reverse-phase high-performance liquid chromatography (HPLC) mass spectrometry (MS). Data were collected in negative mode on a Thermo Exactive mass spectrometer following established methods (35, 36). Intracellular metabolites and the multiple isotopologues produced by the ^{13}C-labeling experiments were identified and quantified using the MAVEN software package (37, 38). The intracellular levels were blank-subtracted using blank samples, which were obtained by filtering the cells out and running the cell-free extracellular medium through the same extraction procedure described above before the LC-MS measurements.

Metabolic flux analysis. Flux distributions under different sugar media were calculated from the following steady-state ^{13}C-labeling experiments: [1,2-$^{13}C_2$]Gluc alone, [U-$^{13}C_6$]Gluc with unlabeled Xyl, unlabeled Gluc with [1,2-$^{13}C_2$]Xyl, [U-$^{13}C_6$]Gluc with unlabeled Arab, unlabeled Gluc with [1-$^{13}C_1$]Arab, [1,2-$^{13}C_2$]Xyl with unlabeled Arab, and unlabeled Xyl with [1-$^{13}C_1$]Arab. We constructed a carbon mapping model to calculate the fluxes through PKP, PPP, and upper glycolysis from the labeling patterns of ribose-5-phosphate (R5P), Xu5P, glucose-6-phosphate (G6P), fructose-1,6-bisphosphate (FBP), dihydroxyacetone-phosphate (DHAP), and 3-phosphoglycerate (3-PG) (see Fig. S2 in the supplemental material). In each experiment, sugar uptake rates were measured using NMR analysis on growth media, and growth rate was used to calculate biomass effluxes from upper glycolysis and the PPP (39, 45). We applied the 13CFLUX2 (http://www.13cflux.net) package (40) to obtain initial flux results as well as to generate cumulative isotopomer networks for further optimization followed by 95% confidence interval estimation as previously described (41). Fluxes were fit to networks, including or lacking one or both of the reactions of the PKP. Comparisons of the match between the estimated labeling data and the measured labeling data are illustrated in Fig. S3 and S4 in the supplemental material.

RESULTS AND DISCUSSION

Growth phenotype and sugar consumption. *C. acetobutylicum* cells grown on Gluc, Gluc:Xyl, Gluc:Arab, and Xyl:Arab showed a doubling time of about 2 to 2.5 h (1.80 ± 0.08, 2.29 ± 0.08, 2.22 ± 0.09 h, and 2.49 ± 0.09, respectively) (Fig. 2A). Thus, a mixture consisting only of pentose sugars was sufficient to promote growth at a rate only slightly slower than growth on glucose. As expected, in the growth medium containing both Gluc and a pentose, the kinetics of the substrate depletion indicated a clear preference for Gluc (Fig. 2B). In the presence of Gluc and Xyl, there was no appreciable depletion of Xyl in the medium, but the Gluc consumption rate (34.4 ± 2.9 mmol C $liter^{-1}$ h^{-1}) was indistinguishable from the uptake rate of Gluc as the sole C source (39.9 ± 5.3 mmol C $liter^{-1}$ h^{-1}) (Fig. 2B). In the presence of Gluc and Arab, the sum of an appreciable, though small, uptake rate of Arab (5.7 ± 1.3 mmol C $liter^{-1}$ h^{-1}) and the Gluc uptake rate (27.6 ± 3.0 mmol C $liter^{-1}$ h^{-1}) approximately equaled the uptake rate of Gluc when the hexose was the only C source (Fig. 2B). This finding implied that the assimilation of carbon from both Gluc and Arab fulfilled the carbon budget requirement of the cells grown on the Gluc:Arab mixture. When the cells were grown on both Xyl and Arab, there was minimal consumption of Xyl, and the uptake rate of Arab (22.0 ± 1.9 mmol C $liter^{-1}$ h^{-1}) was the same as the uptake rate during growth with Arab alone (23.5 ± 1.6 mmol $liter^{-1}$ h^{-1}) (Fig. 2B; see also Fig. S5 in the supplemental material), indicating a preference for Arab over Xyl. In summary, these data show that Gluc is utilized

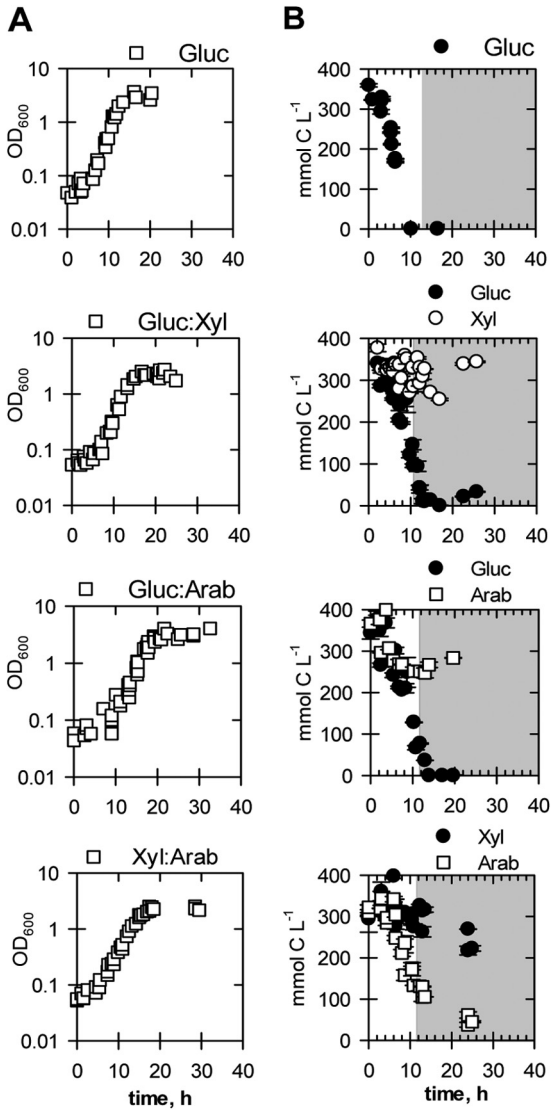

FIG 2 Growth curves (A) and kinetics of substrate depletion (B) during growth of *C. acetobutylicum* on, from top to bottom, glucose (Gluc), glucose:xylose (Gluc:Xyl), glucose:arabinose (Gluc:Arab), and xylose:arabinose (Xyl:Arab); the white and gray areas represent, respectively, the exponential and stationary phases in each growth condition. All the data obtained from biological replicates ($n = 3$ to 5) are shown.

from the growth medium preferentially over the pentose sugars and that Arab is utilized preferentially over Xyl.

Hierarchical intracellular metabolism. In order to probe the link between the preferential consumption of the sugars and their metabolic fates, we investigated the assimilation of the different sugars into intracellular metabolites (Fig. 3 and 4). First, we monitored the incorporation of [U-$^{13}C_6$]Gluc in the absence (as a control) and in the presence of unlabeled Xyl or unlabeled Arab (Fig. 3A). In both Gluc:Xyl and Gluc:Arab mixtures, Xu5P and R5P (PPP intermediates just downstream of the pentose transport step) were 60% to 80% unlabeled, indicating both transport and initial assimilation of these pentose sugars despite the presence of Gluc (Fig. 3A). We also observed that S7P, another PPP intermediate further downstream, was 46% to 60% unlabeled, confirming assimilation of Xyl and Arab through the PPP in the presence of Gluc (Fig. 2A). However, isotopic enrichments of G6P and FBP (upper glycolytic intermediates) were the same as those measured with Gluc alone (Fig. 3A). Similarly, very little pentose-derived carbon was observed in 3-PG, a lower glycolytic intermediate (Fig. 3A). Identical conclusions can be made when the labeling of the substrates were reversed, i.e., unlabeled Gluc with labeled pentoses (Fig. 3B and C). In these labeling experiments, the PPP intermediates were mainly labeled whereas both upper and lower glycolytic metabolites were mostly nonlabeled, further confirming the accumulation of the assimilated (unlabeled) pentoses primarily in PPP (Fig. 3B and C). These labeling patterns thus demonstrate that there was minimal to no flux of the assimilated pentoses in PPP toward glycolysis (Fig. 3A). Accordingly, the lack of apparent Xyl consumption as illustrated in Fig. 2B may be because the rate of its extracellular depletion was so low and not detectable by the NMR technique.

In agreement with the labeling patterns, the intracellular metabolome of *C. acetobutylicum* cells grown on the Gluc:pentose mixtures had an accumulation in PPP metabolites (Fig. 5A and B). However, compared to the PPP metabolites, the concentrations of the glycolytic metabolites did not change coherently (Fig. 5A). Thus, the glycolytic compounds do not cluster together. The upper glycolytic intermediates (G6P, F6P, FBP) measured during growth on Gluc:pentose mixtures were comparable to those measured under Gluc alone, whereas concentrations of the lower glycolytic metabolites (3-PG, DHAP, phosphoenolpyruvate [PEP]) differed for the Gluc:pentose mixtures (Fig. 5C). For Gluc:Xyl growth, 3-PG was the same as during Gluc growth but the lower glycolytic metabolites DHAP and PEP were less; on the other hand, for Gluc:Arab growth, the level of 3-PG was elevated while the PEP level was less, compared to that for Gluc alone (Fig. 5C).

To probe further the aforementioned preferential utilization of Arab over Xyl, we monitored the incorporation of [1,2-$^{13}C_2$]Xyl in the absence (as a control) and presence of unlabeled Arab (Fig. 4A); reverse labeling experiments with unlabeled Xyl and labeled arabinose ([1-$^{13}C_1$]Arab) were also conducted (Fig. 4B). Both labeled and unlabeled forms of PPP and glycolytic intermediates indicated that both Xyl and Arab are incorporated in the intracellular metabolites (Fig. 4). The relatively low levels of isotopic enrichment in the presence of labeled xylose and unlabeled arabinose (20% labeling in the PPP intermediates Xu5P, R5P, and S7P) confirmed a preferential utilization of Arab over Xyl (Fig. 4A); this was further confirmed by the relatively high levels of isotopic enrichment in the presence of unlabeled xylose and labeled arabinose (Fig. 4B). The intracellular metabolome during growth on Xyl:Arab indicated an accumulation in PPP intermediates and depletion in glycolytic metabolites, compared to those for growth on Gluc alone (Fig. 5). Most interestingly, the relatively higher intracellular level of Ac-P in the presence of the pentose sugars suggests involvement of the PKP in metabolism of the pentose-containing sugar mixtures (Fig. 5B).

The main PKP reaction (shown as pk1 in Fig. 6) involves the phosphorylation of the first two carbons of Xu5P to produce Ac-P, with the last three carbons forming GAP. In the steady-state labeling experiments with [1-$^{13}C_1$]arabinose with either unlabeled glucose or unlabeled xylose, there was an enrichment in singly labeled forms (about 80%) on Xu5P (which is primarily the result of the assimilated Arab) compared to that of the nonlabeled forms

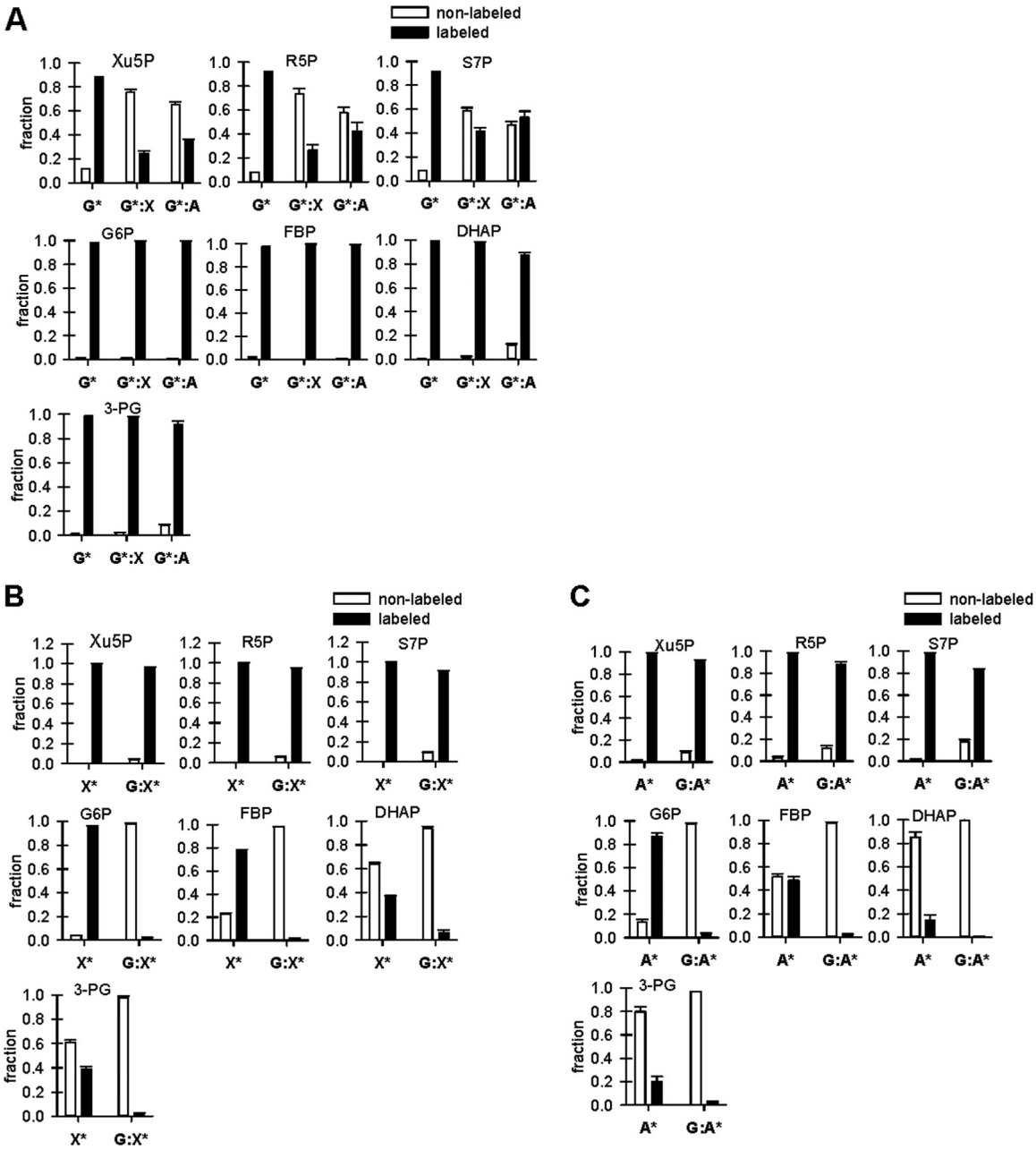

FIG 3 Steady-state isotopic labeling of metabolites in the pentose phosphate and glycolytic pathways following the incorporation of [U-$^{13}C_6$]glucose alone or in the presence of either unlabeled xylose or unlabeled arabinose (A), the incorporation of [1,2-$^{13}C_2$]xylose alone or in the presence of unlabeled glucose (B), and the incorporation of [1-$^{13}C_1$]arabinose alone or in the presence of unlabeled glucose (C). Legend for *x* axis: unlabeled glucose, G; unlabeled xylose, X; unlabeled arabinose, A; labeled glucose, G*; labeled xylose, X*; labeled arabinose, A*. Legend for metabolite names: glucose-6-phosphate, G6P; fructose-1,6-bisphosphate, FBP; dihydroxyacetone-phosphate, DHAP; glyceraldehyde-3-phosphate, GAP; xylulose-5-phosphate, Xu5P; ribose-5-phosphate, R5P; sedoheptulose-7-phosphate, S7P; 3-phosphoglycerate, 3-PG. The data (averages ± standard deviations) were from biological replicates ($n = 3$).

(about 80%) of triose phosphates (DHAP, GAP, 3-PG) (Fig. 6A and B). Therefore, we expect that Ac-P would be largely nonlabeled in the absence of PKP, in which case Ac-P would be derived only from lower glycolysis. However, we measured about 50% (or more) of singly labeled Ac-P, thus providing direct evidence of the involvement of the PKP reaction in the metabolism of both the Gluc:Arab and the Xyl:Arab mixtures (Fig. 6A and B). We note that, during growth on the pentose mixture, routing of the assimilated pentoses toward glycolysis via only PPP would produce both singly and doubly ^{13}C-labeled forms of triose-phosphates in addition to nonlabeled forms (Fig. 6B), but fluxes through PKP would result in an increased amount of nonlabeled forms of triose phosphates. Consistent with fluxes through PKP, the measured labeling patterns showed that the nonlabeled forms of FBP and triose-phosphates were more than twice those of pentose-phosphates and G6P (Fig. 6B). Thus, our metabolomics and labeling data confirm selective utilization of Arab over Xyl from sugar mixtures with subsequent catabolism via the PKP. The relative

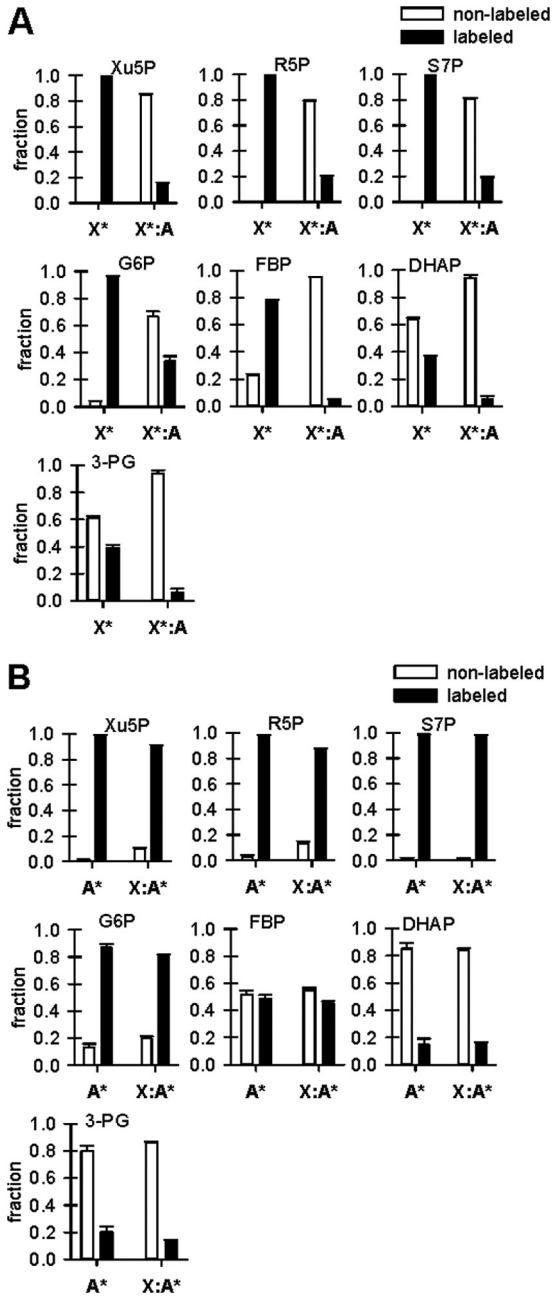

FIG 4 Steady-state isotopic labeling of metabolites in the pentose phosphate and glycolytic pathways following the incorporation of [1,2-$^{13}C_2$]xylose alone or in the presence of unlabeled arabinose (A) and the incorporation of [1-$^{13}C_1$]arabinose alone or in the presence of unlabeled xylose (B). Legend for *x* axis: unlabeled xylose, X; unlabeled arabinose, A; labeled xylose, X*; labeled arabinose, A*. Legend for metabolite names: glucose-6-phosphate, G6P; fructose-1,6-bisphosphate, FBP; dihydroxyacetone-phosphate, DHAP; glyceraldehyde-3-phosphate, GAP; xylulose-5-phosphate, Xu5P; ribose-5-phosphate, R5P; sedoheptulose-7-phosphate, S7P; 3-phosphoglycerate, 3-PG. The data (averages ± standard deviations) were from biological replicates ($n = 3$).

metabolic fluxes through PKP and PPP/glycolysis in mixed-sugar metabolism have, however, not yet been quantified.

Quantitative metabolic flux analysis. It is challenging to understand the fluxes of metabolic pathways only by visual examination of labeling data, especially due to the reversibility of the reactions in PPP. In order to explore quantitatively the apparent hierarchical metabolism of the different sugars, we employed a metabolic network model to analyze the metabolic flux through PPP, PKP, and glycolysis (Fig. 7A). In a previous analysis of the involvement of PKP during Xyl metabolism in *C. acetobutylicum*, only one of the PK reactions involving the conversion of Xu5P to Ac-P and GAP was included (Fig. 7A) (35). We examine here also the other PK reaction, which converts F6P to Ac-P and E4P (Fig. 7A) (5). In order to determine the relative importance of the two PK reactions in the PKP, we performed our MFA analysis in the absence and presence of both PK reactions as well as in the presence of only one of them at a time; Fig. 7B reports the overall deviation of the model estimates from the measured labeling patterns. The model could not adequately fit the experimental labeling data when both PKP reactions were excluded, with either reaction generally sufficient to fit the observed data except in the cases of the Gluc:Arab mixture, in which the phosphoketolase 1 (PK1) reaction was necessary, and of the Gluc:Xyl mixture, in which the phosphoketolase 2 (PK2) reaction was necessary (Fig. 7B; see also Fig. S3 and S4 in the supplemental material). Therefore, we included both PK1 and PK2 reactions in the model network for the estimation of the quantitative fluxes of sugar metabolism for all growth conditions (Fig. 7C, D, and E).

The estimated uptake rates of the quantitative flux analysis agree well with the measured uptake rates (Fig. 7C). During growth on Gluc, Gluc:Xyl, and Gluc:Arab, the fluxes through upper glycolytic reactions (glucose-6-phosphate isomerase [PGI], phosphofructokinase [PFK], fructose-bisphosphate aldolase [FPA], triphosphate-isomerase [TPI]) were similar (on average, about 12.6 to 16.1 mmol $g_{CDW}^{-1}\ h^{-1}$ [where g_{CDW} is the cell dry weight in grams]) because they were driven mostly by the uptake rate of Gluc (Fig. 7C and D). Expectedly, the flux through glyceraldehyse-3-phosphate dehydrogenase (GAPDH) equated the sum of the fluxes through FBA and TPI. The very low fluxes (on average, less than 0.2 mmol $g_{CDW}^{-1}\ h^{-1}$) through the PPP reactions (ribulose-5-phosphate-3-epimerase [RPE], transketolase 1 [TK1], transketolase 2 [TK2], transaldolase [TAL]) indicated that, despite the observed accumulation of PPP intermediates in cells grown on Gluc:pentose mixtures, there was minimal flux through the PPP to glycolysis (Fig. 7D and E). In terms of the role of PKP, comparable low fluxes (about 0.1 to 0.9 mmol $g_{CDW}^{-1}\ h^{-1}$) of both PK1 and PK2 were estimated during growth on Gluc and Gluc:Xyl, but the metabolism of Gluc:Arab resulted in a PK1 flux and a PK2 flux of up to 3.8 mmol $g_{CDW}^{-1}\ h^{-1}$ each (Fig. 7E). The relatively higher PK fluxes during the metabolism of Gluc:Arab is consistent with the higher unlabeled fraction observed for 3-PG in the presence of labeled Gluc:unlabeled Arab than in the presence of labeled Gluc:unlabeled Xyl (Fig. 6A).

In contrast to the Gluc:pentose mixtures, fluxes through upper glycolysis were much less (about 2.6 mmol $g_{CDW}^{-1}\ h^{-1}$ or less) during growth on Xyl:Arab, consistent with the requirement that fluxes through lower glycolysis and PKP be fed primarily from PPP under this growth condition (Fig. 7D). The higher flux of GAP to 3-PG via GAPDH than the sum of FBA and TPI reflects the PK1 reaction flux contribution during growth on the pentose mixture (Fig. 7D), with the model fit predicting significant fluxes via both PK1 and PK2, with the former being more than twice the value of the latter (on average, 9.8 mmol $g_{CDW}^{-1}\ h^{-1}$ and 2.6 mmol $g_{CDW}^{-1}\ h^{-1}$, respectively) (Fig. 7E). Based on the flux out of Ac-P (which may flow to either acetate or acetyl-CoA) in the flux

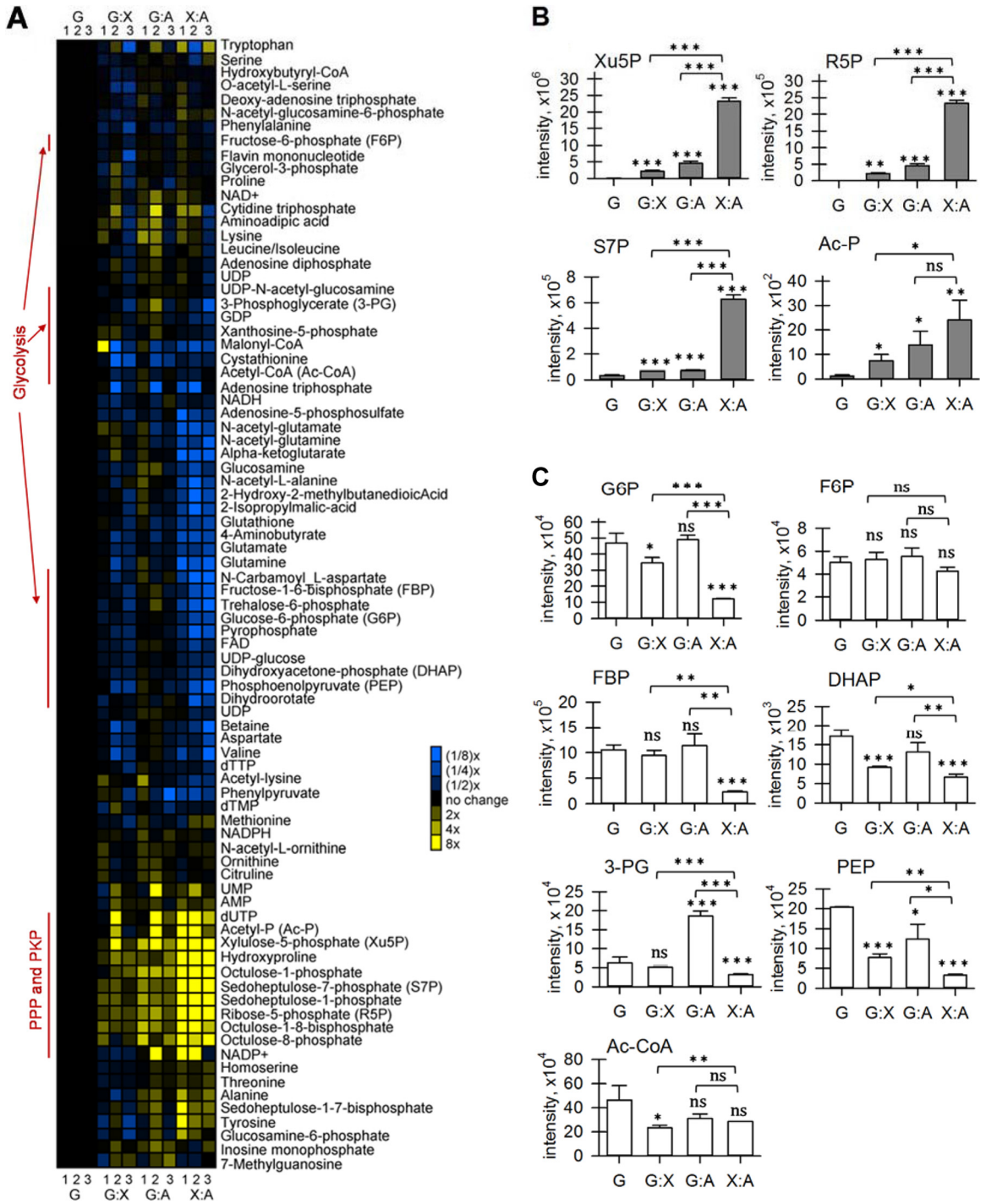

FIG 5 Unsupervised hierarchical clustering of the intracellular metabolome (A) and intracellular levels of pentose phosphate pathway (PPP) and phosphoketolase pathway (PKP) metabolites (B) and glycolytic metabolites (C) obtained during exponential growth of C. *acetobutylicum* on glucose (G), glucose:xylose (G:X), glucose:arabinose (G:A), and xylose:arabinose (X:A). In panel A, amounts are shown relative to levels in cells grown on glucose alone; columns 1, 2, and 3 represent results from three experiments involving different starting colonies of *C. acetobutylicum* and different days of analysis. For each column, results are averages from three biological replicates grown in parallel from the same starting colony. In panels B and C, intensity levels are from liquid chromatography-mass spectrometry measurements (averaged values ± standard deviations) from three biological replicates from one starting colony; the data for the other two starting colonies are shown in Fig. S6 in the supplemental material (comparison of raw mass spectrometry intensity values across starting colonies is inappropriate due to day-to-day drift in mass spectrometer detector response factor). Two-tailed unpaired *t* test analysis comparing the intensity levels measured during growth on the mixtures versus growth on Gluc alone (bottom statistics) and comparing intensity levels during growth on the pentose mixture versus the glucose:pentose mixtures (upper statistics): ***, $P < 0.001$; **, $P < 0.01$; *, $P < 0.05$; ns, not statistically significant.

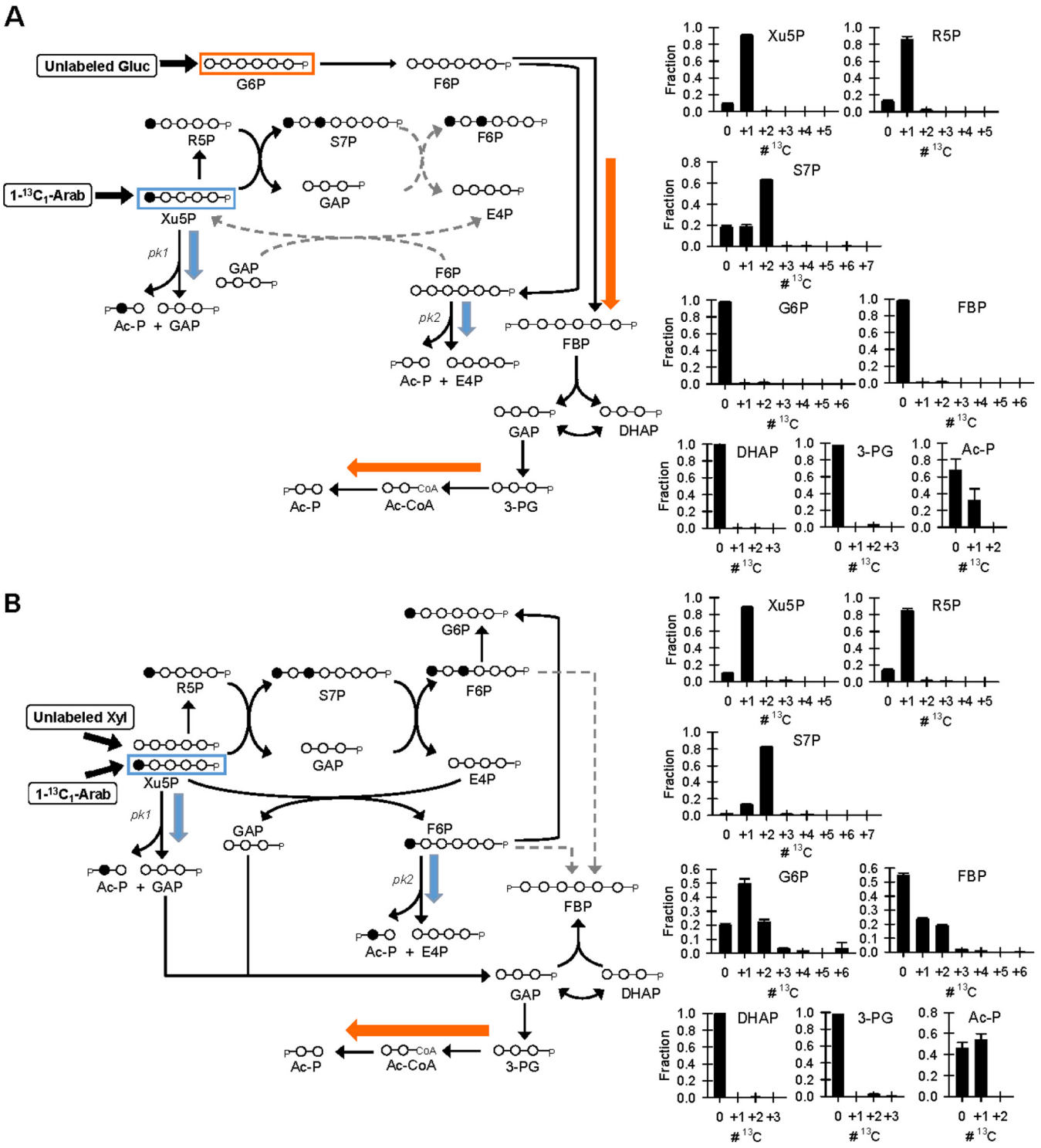

FIG 6 Carbon mapping (left) and measured isotopologue distribution of labeled intracellular metabolites (right) following steady-state incorporation of unlabeled glucose with [1-$^{13}C_1$]arabinose (A) and unlabeled xylose with [1-$^{13}C_1$]arabinose (B). The carbon mapping with black arrows is focused on the catabolism of the major isotopomer forms through the primary metabolic reactions of PKP, PPP, and glycolysis. The broken-lined gray arrows indicate the formation of minor isotopologue forms. The blue and orange arrows indicate the formation of acetyl-phosphate via phosphoketolase reaction and lower glycolysis, respectively. Legend for metabolite names: glucose-6-phosphate, G6P; fructose-6-phosphate, F6P; fructose-1,6-bisphosphate, FBP; dihydroxyacetone-phosphate, DHAP; glyceraldehyde-3-phosphate, GAP; xylulose-5-phosphate, Xu5P; ribose-5-phosphate, R5P; sedoheptulose-7-phosphate, S7P; 3-phosphoglycerate, 3-PG; acetyl-phosphate, Ac-P; and acetyl-coenzyme A (Ac-CoA). The measured data (averages ± standard deviations) were from biological replicates ($n = 3$).

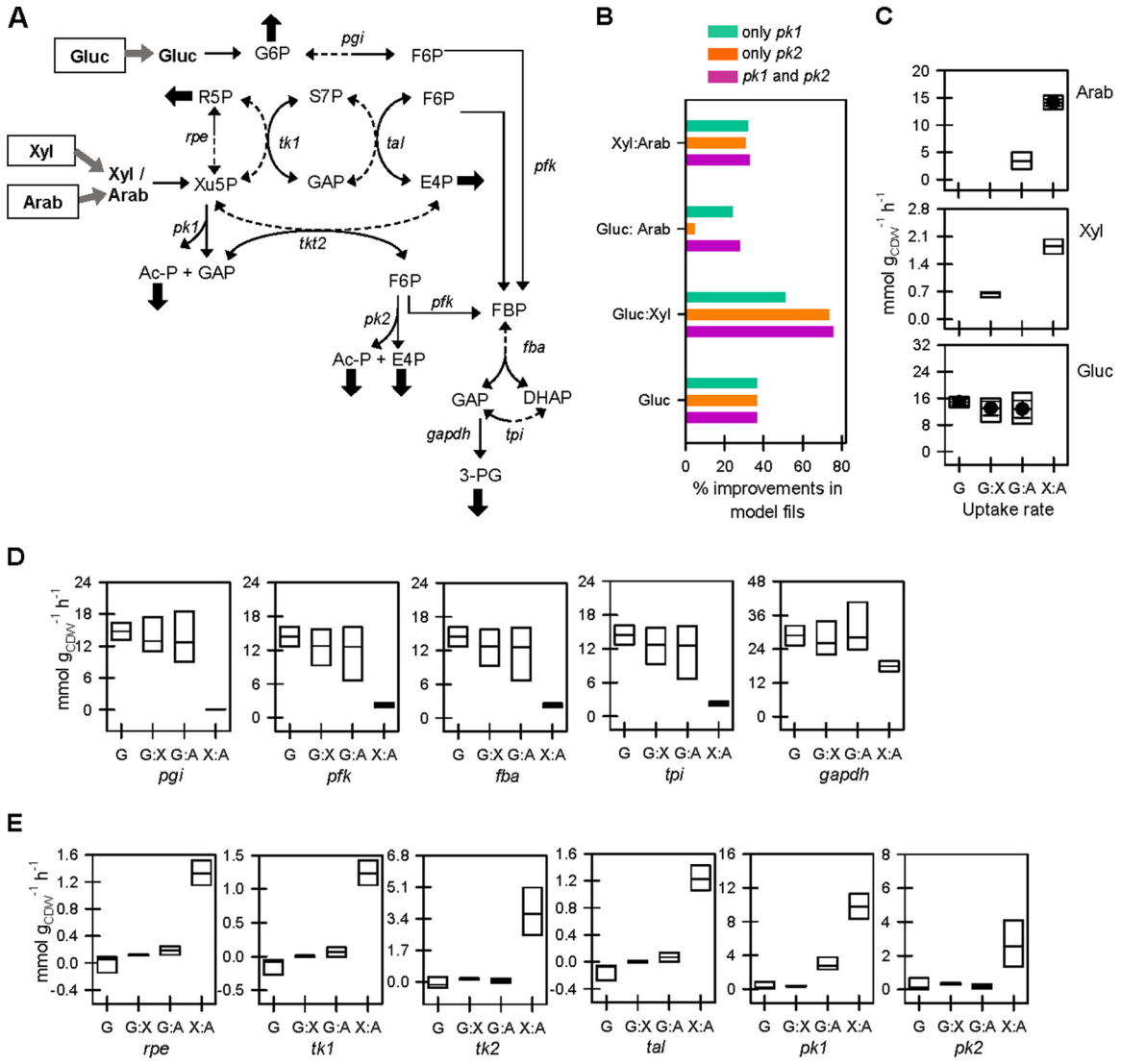

FIG 7 Model metabolic network (A), model improvements following incorporation of both or one of the phosphoketolase reactions relative to the absence of these reactions (B), and fluxes estimated for uptake rate (C), reactions in glycolysis (D), and reactions in pentose phosphate and phosphoketolase pathways (E) during *C. acetobutylicum* growth on glucose (G), glucose:xylose (G:X), glucose:arabinose (G:A), and xylose:arabinose (X:A). In panel A, solid and dotted thin black arrows represent forward and backward directions of the metabolic reactions, respectively; gray and black thick arrows represent uptake steps and excretion steps, respectively. In panel B, the model improvements were determined from the variance-weighted sum of residuals following the metabolic flux modeling with only PK1 (green), only PK2 (orange), and both PK1 and PK2 (purple); the absolute values for each condition are shown in Fig. S7 in the supplemental material. In panel C, the measured fluxes (averages ± standard deviations) are shown as data points with error bars. In panels C to E, the estimated fluxes from the modeled metabolic network, including both PK reactions, are shown as box plots wherein the bars represent the mean values and the height of the box indicates the span of the 95% confidence intervals. Legend for enzymes: glucose-6-phosphate isomerase, pgi; phosphofructokinase, pfk; ribulose-5-phosphate-3-epimerase, rpe; transketolase 1, tk1; transketolase 2, tk2; transaldolase, tal; phosphoketolase, pk1; phosphoketolase 2, pk2; fructose-bisphosphate aldolase, fba; triphosphate isomerase, tpi; glyceraldehyde-3-phosphate dehydrogenase, gapdh.

model (Fig. 7A), we estimated that the total PKP flux was, on average, 2.0%, 4.7%, 22.1%, and 79.1% of the total influx of carbon consumption from Gluc, Gluc:Xyl, Gluc:Arab, and Xy:Arab, respectively. Our MFA thus revealed that, in the mixtures, PKP activity was minimal in the presence of Gluc but contributed significantly to the catabolism of pentoses when Gluc was absent and especially in the presence of Arab. In essence, the glycolytic fluxes are replaced largely by PKP fluxes in the absence of Gluc. Liu et al. (13) reported that Xyl catabolic flux through the PKP in *C. acetobutylicum* increases with increasing Xyl concentration. Our data indicated that the PKP flux increased with pentose uptake from the Gluc:pentose mixtures, with Arab both more preferred as a C source and more strongly inducing PKP flux than Xyl.

Implications for acid and solvent production. Our results thus far indicate that Arab is critical to inducing phosphoketolase enzyme and flux. Increased flux via PKP has been implicated in increasing acetate production during growth on Arab alone, and the expression of the phosphoketolase enzyme was highly induced in the presence of Arab alone, compared to Gluc or Xyl alone (5). In order to examine the consequence of the hierarchical metabolism of sugar mixtures on acidogenesis and solventogenesis, we measured the extracellular amount of the acids (acetate and bu-

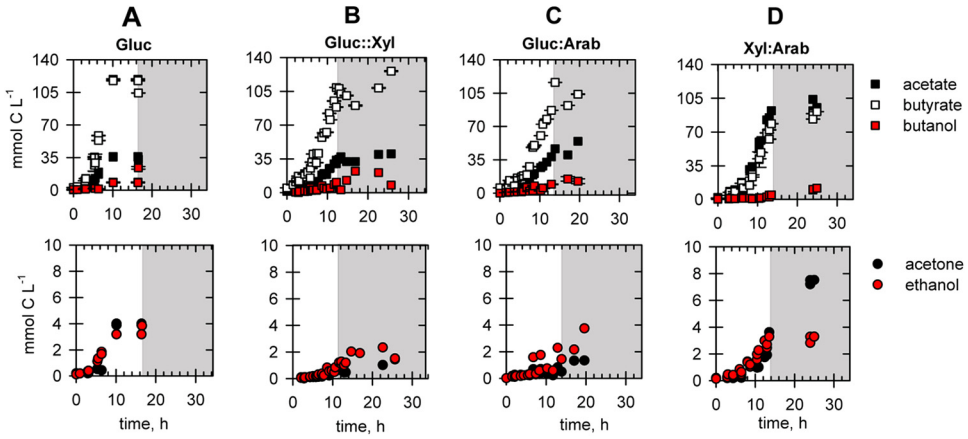

FIG 8 Kinetics of extracellular levels of acids (butyrate, acetate) and solvents (butanol, acetone, ethanol) during *C. acetobutylicum* growth on glucose (Gluc) (A), glucose:xylose (Gluc:Xyl) (B), glucose:arabinose (Gluc:Arab) (C), and xylose:arabinose (Xyl:Arab) (D); the white and gray areas represent, respectively, the exponential and stationary phases in each growth condition. All experimental data obtained from biological replicates ($n = 3$) are shown.

tyrate) and solvents (butanol, ethanol, and acetone) secreted by *C. acetobutylicum* in response to the different sugar growth conditions. Consistent with Gluc being the dominant sugar consumed in the Gluc:pentose mixtures, the amounts of acids and solvents produced during growth on Gluc:Xyl or on Gluc:Arab (from an initial concentration of 660 mmol C liter^{-1} at 50:50 Gluc:pentose) were similar to the amounts produced from Gluc alone (with initial concentration of 330 mmol C liter^{-1}) (Fig. 8A, B, and C). These results are consistent with a lack of efficient metabolism of the pentose sugar, to yield an additive production of acids and solvents. In contrast to growth on Gluc and Gluc:pentose mixtures, growth on Xyl:Arab yielded significantly more acids and also more acetone in the extracellular medium (Fig. 8). Specifically, there was a 3-fold increase in acetate production (which is readily explained based on the PKP flux) and more than two times more acetone generated [perhaps as a redox-neutral means of disposing of acetyl-CoA; unlike ethanol, acetone excretion does not require NAD(P)H] (Fig. 1B and 8D).

Our findings demonstrate that hexose and pentose sugars have different metabolic fates when *C. acetobutylicum* is grown on both types of sugars. Hexoses dominate glycolysis and support glycolytically derived acidogenesis and solventogenesis, whereas pentoses accumulate in PPP, presumably to feed ribonucleotide synthesis, and also supply carbon to the PKP toward increasing acetate production. In addition to carbon catabolite repression (15, 16), hierarchical metabolism may be a common strategy in bacteria in an effort to adapt to different nutritional environments (30). For instance, cocatabolism of carbon substrates in *Mycobacterium tuberculosis*, a pathogenic aerobic bacterium, exhibited a hierarchical metabolic fate that optimizes carbon utilization for bacterial growth (30). The involvement of PKP in *C. acetobutylicum* provides a nonoxidative pathway which can yield greater carbon conservation from F6P and Xu5P to acetyl-CoA by bypassing the one-carbon loss during the conversion of pyruvate to acetyl-CoA (42) (Fig. 1B). Increased expression of PKP-involved enzymes may be a potential bioengineering avenue to enhance pentose catabolism from Gluc:pentose mixtures in soil *Clostridia*. To make a practical bioengineering contribution, however, it will be necessary to avoid loss of the Ac-P generated by the PKP as acetate and instead direct it into acetyl-CoA and thus production of solvents or other more valuable products.

ACKNOWLEDGMENTS

This work was funded by grant DE-FG02-07ER64488 from the United States Department of Energy (DOE). L.A. acknowledges a postdoctoral fellowship from the National Science Foundation (NSF).

We thank Wenyun Lu, Jing Fan, Meytal B. Higgins, Jurre Kamphorst, and Daniel Amador-Noguez for assistance during the LC-MS measurements and helpful discussions during the performance of this research and István Pelczer for technical assistance during the NMR measurements. We thank two anonymous reviewers for their insightful comments.

REFERENCES

1. **Dürre P.** 1998. New insights and novel developments in clostridial acetone/butanol/isopropanol fermentation. Appl Microbiol Biotechnol **49:** 639–648. http://dx.doi.org/10.1007/s002530051226.
2. **Desai RP, Harris LM, Welker NE, Papoutsakis ET.** 1999. Metabolic flux analysis elucidates the importance of the acid formation pathways in regulating solvent production by *Clostridium acetobutylicum*. Metab Eng **1:**206–213. http://dx.doi.org/10.1006/mben.1999.0118.
3. **Hu S, Zheng H, Gu Y, Zhao J, Zhang W, Yang Y, Wang S, Zhao G, Yang S, Jiang W.** 2011. Comparative genomic and transcriptomic analysis revealed genetic characteristics related to solvent formation and xylose utilization in *Clostridium acetobutylicum* EA 2018. BMC Genomics **12:**93. http://dx.doi.org/10.1186/1471-2164-12-93.
4. **Ren C, Gu Y, Hu S, Wu Y, Wang P, Yang Y, Yang C, Yang S, Jiang W.** 2010. Identification and inactivation of pleiotropic regulator CcpA to eliminate glucose repression of xylose utilization in *Clostridium acetobutylicum*. Metab Eng **12:**446–454. http://dx.doi.org/10.1016/j.ymben.2010.05.002.
5. **Servinsky MD, Germane KL, Liu S, Kiel JT, Clark AM, Shankar J, Sund CJ.** 2012. Arabinose is metabolized via a phosphoketolase pathway in *Clostridium acetobutylicum* ATCC 824. J Ind Microbiol Biotechnol **39:** 1859–1867. http://dx.doi.org/10.1007/s10295-012-1186-x.
6. **Gheshlagi R, Scharer JM, Moo-Young M, Chou CP.** 2009. Metabolic pathways of clostridia for producing butanol. Biotechnol Adv **27:**764–781. http://dx.doi.org/10.1016/j.biotechadv.2009.06.002.
7. **Grupe H, Gottschalk G.** 1992. Physiological events in *Clostridium acetobutylicum* during the shift from acidogenesis to solventogenesis in continuous culture and presentation of a model for shift induction. Appl Environ Microbiol **58:**3896–3902.
8. **Lee SY, Park JH, Jang SH, Nielsen LK, Kim J, Jung KS.** 2008. Fermentative butanol production by clostridia. Biotechnol Bioeng **101:**209–228. http://dx.doi.org/10.1002/bit.22003.
9. **Sun Y, Cheng J.** 2002. Hydrolysis of lignocellulosic materials for ethanol production: a review. Bioresour Technol **83:**1–11. http://dx.doi.org/10.1016/S0960-8524(01)00212-7.
10. **Amador-Noguez D, Feng XJ, Fan J, Roquet N, Rabitz H, Rabinowitz JD.** 2010. Systems-level metabolic flux profiling elucidates a complete,

bifurcated tricarboxylic acid cycle in *Clostridium acetobutylicum*. J Bacteriol **192:**4452–4461. http://dx.doi.org/10.1128/JB.00490-10.
11. **Amador-Noguez D, Brasg IA, Feng X-J, Roquet N, Rabinowitz JD.** 2011. Metabolome remodeling during the acidogenic-solventogenic transition in *Clostridium acetobutylicum*. Appl Environ Microbiol **77:**7984–7997. http://dx.doi.org/10.1128/AEM.05374-11.
12. **Servinsky MD, Kiel JT, Dupuy NF, Sund CJ.** 2010. Transcriptional analysis of differential carbohydrate utilization by *Clostridium acetobutylicum*. Microbiology **156:**3478–3491. http://dx.doi.org/10.1099/mic.0.037085-0.
13. **Liu L, Zhang L, Tang W, Gu Y, Hua Q, Yang S, Jiang W, Yang C.** 2012. Phosphoketolase pathway for xylose catabolism in *Clostridium acetobutylicum* revealed by ^{13}C metabolic flux analysis. J Bacteriol **194:**5413–5422. http://dx.doi.org/10.1128/JB.00713-12.
14. **Fond O, Engasser J-M, Matta-El-Amouri G, Petitdemange H.** 1986. The acetone butanol fermentation on glucose and xylose. I. Regulation and kinetics in batch cultures. Biotechnol Bioeng **28:**160–166.
15. **Grimmler C, Held C, Liebl W, Ehrenreich A.** 2010. Transcriptional analysis of catabolite repression in *Clostridium acetobutylicum* growing on mixtures of D-glucose and D-xylose. J Biotechnol **150:**315–323. http://dx.doi.org/10.1016/j.jbiotec.2010.09.938.
16. **Ounine K, Petitdemange H, Raval G, Gay R.** 1985. Regulation and butanol inhibition of D-xylose and D-glucose uptake in *Clostridium acetobutylicum*. Appl Environ Microbiol **49:**874–878.
17. **Ounine K, Petitdemange H, Raval G, Gay R.** 1983. Acetone-butanol production from pentoses by *Clostridium acetobutylicum*. Biotechnol Lett **5:**605–610. http://dx.doi.org/10.1007/BF00130841.
18. **Gu Y, Li J, Zhang L, Chen J, Niu L, Yang Y, Yang S, Jiang W.** 2009. Improvement of xylose utilization in *Clostridium acetobutylicum* via expression of the *talA* gene encoding transaldolase from *Escherichia coli*. J Biotechnol **43:**284–287. http://dx.doi.org/10.1016/j.jbiotec.2009.08.009.
19. **Xin F, Wu YR, He J.** 2014. Simultaneous fermentation of glucose and xylose to butanol by *Clostridium* sp. strain BOH3. Appl Environ Microbiol **80:**4771–4778. http://dx.doi.org/10.1128/AEM.00337-14.
20. **Blencke HM, Homuth G, Ludwig H, Mäder U, Hecker M, Stülke J.** 2003. Transcriptional profiling of gene expression in response to glucose in *Bacillus subtilis*: regulation of the central metabolic pathways. Metab Eng **5:**133–149. http://dx.doi.org/10.1016/S1096-7176(03)00009-0.
21. **Küster E, Hilbich T, Dahl MK, Hillen W.** 1999. Mutations in catabolite control protein CcpA separating growth effects from catabolite repression. J Bacteriol **181:**4125–4128.
22. **Singh KD, Schmalisch MH, Stülke J, Görke B.** 2008. Carbon catabolite repression in *Bacillus subtilis*: quantitative analysis of repression exerted by different carbon sources. J Bacteriol **190:**7275–7284. http://dx.doi.org/10.1128/JB.00848-08.
23. **Xiao H, Gu Y, Ning Y, Yang Y, Mitchell WJ, Jiang W, Yang S.** 2011. Confirmation and elimination of xylose metabolism bottlenecks in glucose phosphoenolpyruvate-dependent phosphotransferase system-deficient *Clostridium acetobutylicum* for simultaneous utilization of glucose, xylose, and arabinose. Appl Environ Microbiol **77:**7886–7895. http://dx.doi.org/10.1128/AEM.00644-11.
24. **Dunn WB, Bailey NJ, Johnson HE.** 2005. Measuring the metabolome: current analytical technologies. Analyst **130:**606–625. http://dx.doi.org/10.1039/b418288j.
25. **Kwon YK, Higgins MB, Rabinowitz JD.** 2010. Antifolate-induced depletion of intracellular glycine and purines inhibits thymineless death in *E. coli*. ACS Chem Biol **5:**787–795. http://dx.doi.org/10.1021/cb100096f.
26. **Lindon JC, Nicholson JK, Holmes E, Keun HC, Craig A, Pearce JT, Bruce SJ, Hardy N, Sansone SA, Antti H, Jonsson P, Daykin C, Navarange M, Beger RD, Verheij ER, Amberg A, Baunsgaard D, Cantor GH, Lehman-McKeeman L, Earll M, Wold S, Johansson E, Haselden JN, Kramer K, Thomas C, Lindberg J, Schuppe-Koistinen I, Wilson ID, Reily MD, Robertson DG, Senn H, Krotzky A, Kochhar S, Powell J, van der Ouderaa F, Plumb R, Schaefer H, Spraul M, Standard Metabolic Reporting Structures Working Group.** 2005. Summary recommendations for standardization and reporting of metabolic analyses. Nat Biotechnol **23:**833–838. http://dx.doi.org/10.1038/nbt0705-833.
27. **Monot F, Martin JR, Petitdemange H, Gay R.** 1982. Acetone and butanol production by *Clostridium acetobutylicum* in a synthetic medium. Appl Environ Microbiol **44:**1318–1324.
28. **Nielsen J, Oliver S.** 2005. The next wave in metabolome analysis. Trends Biotechnol **23:**544–546. http://dx.doi.org/10.1016/j.tibtech.2005.08.005.
29. Reference deleted.
30. **de Cavalho LPS, de Carvalho LP, Fischer SM, Marrero J, Nathan C, Ehrt S, Rhee KY.** 2010. Metabolomics of *Mycobacterium tuberculosis* reveals compartmentalized co-catabolism of carbon substrates. Chem Biol **17:**1122–1131. http://dx.doi.org/10.1016/j.chembiol.2010.08.009.
31. Reference deleted.
32. **Hwang TL, Shaka AJ.** 1995. Water suppression that works: excitation sculpting using arbitrary wave-forms and pulsed-field gradients. J Magn Reson **112:**275–279. http://dx.doi.org/10.1006/jmra.1995.1047.
33. **Lewis IA, Schommer SC, Markley JL.** 2009. rNMR: open source software for identifying and quantifying metabolites in NMR spectra. Magn Reson Chem **47:**S123–S126. http://dx.doi.org/10.1002/mrc.2526.
34. **Kimball E, Rabinowitz JD.** 2006. Identifying decomposition products in extracts of cellular metabolites. Anal Biochem **358:**273–280. http://dx.doi.org/10.1016/j.ab.2006.07.038.
35. **Lu W, Bennett B, Rabinowitz JD.** 2008. Analytical strategies for LC-MS-based targeted metabolomics. J Chromatogr B Anal Technol Biomed Life Sci **871:**236–242. http://dx.doi.org/10.1016/j.jchromb.2008.04.031.
36. **Lu W, Clasquin MF, Melamud E, Amador-Noguez D, Caudy AA, Rabinowitz JD.** 2010. Metabolomic analysis via reversed-phase ion-pairing liquid chromatography coupled to a stand alone OrbiTrap mass spectrometer. Anal Chem **82:**3212–3221. http://dx.doi.org/10.1021/ac902837x.
37. **Clasquin M, Melamud E, Rabinowitz JD.** 2012. LC-MS data processing with MAVEN: a metabolomic analysis and visualization engine. Curr Protoc Bioinform Chapter **14:**Unit14.11. http://dx.doi.org/10.1002/0471250953.bi1411s37.
38. **Melamud E, Vastag L, Rabinowitz JD.** 2010. Metabolomic analysis and visualization engine for LC-MS data. Anal Chem **82:**9818–9826. http://dx.doi.org/10.1021/ac1021166.
39. **Lee J, Yun H, Feist AM, Palsson BØ, Lee SY.** 2008. Genome-scale reconstruction and in silico analysis of the *Clostridium acetobutylicum* ATCC 824 metabolic network. Appl Microbiol Biotechnol **80:**849–862. http://dx.doi.org/10.1007/s00253-008-1654-4.
40. **Weitzel M, Nöh K, Dalman T, Niedenführ S, Stute B, Wiechert W.** 2013. 13CFLUX2—high-performance software suite for ^{13}C-metabolic flux analysis. Bioinformatics **29:**143–145. http://dx.doi.org/10.1093/bioinformatics/bts646.
41. **Antoniewicz MR, Kelleher JK, Stephanopoulos G.** 2006. Determination of confidence intervals of metabolic fluxes estimated from stable isotope measurements. Metab Eng **8:**324–337. http://dx.doi.org/10.1016/j.ymben.2006.01.004.
42. **Bogorad IW, Lin T-S, Liao JC.** 2013. Synthetic non-oxidative glycolysis enables complete carbon conservation. Nature **502:**693–697. http://dx.doi.org/10.1038/nature12575.
43. **Hollywood K, Brison DR, Goodacre R.** 2006. Metabolomics: current technologies and future trends. Proteomics **6:**4716–4723. http://dx.doi.org/10.1002/pmic.200600106.
44. Reference deleted.
45. **Nölling J, Breton G, Omelchenko MV, Makarova KS, Zeng Q, Gibson R, Lee HM, Dubois J, Qiu D, Hitti J, Wolf YI, Tatusov RL, Sabathe F, Doucette-Stamm L, Soucaille P, Daly MJ, Bennett GN, Koonin EV, Smith DR.** 2001. Genome sequence and comparative analysis of the solvent-producing bacterium *Clostridium acetobutylicum*. J Bacteriol **183:**4823–4838. http://dx.doi.org/10.1128/JB.183.16.4823-4838.2001.
46. **Rabinowitz JD, Kimball E.** 2007. Acidic acetonitrile for cellular metabolome extraction from *Escherichia coli*. Anal Chem **79:**6167–6173. http://dx.doi.org/10.1021/ac070470c.